

Resonant microwaves probing acoustic waves from an RF plasma jet

Citation for published version (APA):

Platier, B., Staps, T. J. A., Hak, C. C. J. M., Beckers, J., & IJzerman, W. L. (2020). Resonant microwaves probing acoustic waves from an RF plasma jet. *Plasma Sources Science and Technology*, 29(4), Article 045024. <https://doi.org/10.1088/1361-6595/ab7d8e>

Document license:

CC BY

DOI:

[10.1088/1361-6595/ab7d8e](https://doi.org/10.1088/1361-6595/ab7d8e)

Document status and date:

Published: 17/04/2020

Document Version:

Publisher's PDF, also known as Version of Record (includes final page, issue and volume numbers)

Please check the document version of this publication:

- A submitted manuscript is the version of the article upon submission and before peer-review. There can be important differences between the submitted version and the official published version of record. People interested in the research are advised to contact the author for the final version of the publication, or visit the DOI to the publisher's website.
- The final author version and the galley proof are versions of the publication after peer review.
- The final published version features the final layout of the paper including the volume, issue and page numbers.

[Link to publication](#)

General rights

Copyright and moral rights for the publications made accessible in the public portal are retained by the authors and/or other copyright owners and it is a condition of accessing publications that users recognise and abide by the legal requirements associated with these rights.

- Users may download and print one copy of any publication from the public portal for the purpose of private study or research.
- You may not further distribute the material or use it for any profit-making activity or commercial gain
- You may freely distribute the URL identifying the publication in the public portal.

If the publication is distributed under the terms of Article 25fa of the Dutch Copyright Act, indicated by the "Taverne" license above, please follow below link for the End User Agreement:

www.tue.nl/taverne

Take down policy

If you believe that this document breaches copyright please contact us at:

openaccess@tue.nl

providing details and we will investigate your claim.

PAPER • OPEN ACCESS

Resonant microwaves probing acoustic waves from an RF plasma jet

To cite this article: B Platier *et al* 2020 *Plasma Sources Sci. Technol.* **29** 045024

View the [article online](#) for updates and enhancements.



IOP | ebooks™

Bringing together innovative digital publishing with leading authors from the global scientific community.

Start exploring the collection—download the first chapter of every title for free.

Resonant microwaves probing acoustic waves from an RF plasma jet

B Platier¹ , T J A Staps¹ , C C J M Hak², J Beckers¹  and W L IJzerman^{3,4}

¹Elementary Processes in Gas Discharges Group, Department of Applied Physics, Eindhoven University of Technology, PO Box 513, 5600 MB Eindhoven, The Netherlands

²Building Acoustics, Department of the Built Environment, Eindhoven University of Technology, PO Box 513, 5600 MB Eindhoven, The Netherlands

³CASA, Department of Mathematics and Computer Science, Eindhoven University of Technology, PO Box 513, 5600 MB Eindhoven, The Netherlands

⁴Signify, High Tech Campus 7, 5656AE Eindhoven, The Netherlands

E-mail: b.platier@tue.nl

Received 9 December 2019, revised 23 February 2020

Accepted for publication 6 March 2020

Published 17 April 2020



CrossMark

Abstract

Microwave cavity resonance spectroscopy is introduced and demonstrated as a new approach to investigate the generation of acoustic waves by a pulsed radio-frequency driven atmospheric-pressure plasma jet. Thanks to recent advancements in the diagnostic method, the lower detection limit for pressure changes in air is ~ 0.3 Pa. Good agreement with conventional pressure transducer measurements with respect to the temporal evolution, the pressure amplitude and the spectral response is found. Fourier analysis revealed that the acoustic waves induced by the plasma can most likely be attributed to standing waves in the discharge geometry. Additionally, the plasma-induced acoustic waves of a few (tens of) Pa are proposed as an active mechanism in plasma medicine.

Keywords: microwave cavity resonance spectroscopy, atmospheric pressure plasma jet, acoustic wave, cavity

1. Introduction

Atmospheric-pressure plasma jets have proven themselves in various industrial applications such as plasma-assisted cleaning and coating [1], deposition [2] and sterilization [3]. Additionally, these sources have shown enormous potential in plasma medicine: e.g. wound healing [4], gene transfection [5] and cancer treatment [6]. The presence of reactive species and the generation of UV radiation, charged particles and electric fields give these plasmas an edge over more conventional technologies [7].

In the last few years the community has started to investigate plasma-induced flow changes in atmospheric-pressure jets. Near the powered electrode, gas heating occurs almost instantaneously, which increases the pressure locally

and subsequently induces acoustic waves [8]. These acoustic waves are a cause for instabilities and disturbances in the flow downstream and directly influence the production of reactive species by the plasma. Despite the importance of the flow for the plasma chemistry and the ability to deliver the species to the target to be treated, the influence of discharges on the gas flow of plasma jets has only been investigated in a few works [9]. Methods used to elucidate this interaction are numerical calculations [8], Schlieren photography [10], optical emission spectroscopy [11] and electrical studies [11].

In this communication, microwave cavity resonance spectroscopy (MCRS) is introduced as a new diagnostic method to study pressure waves. In the original method, a change in resonant behaviour of a standing wave in a cavity—a void enclosed by conductive walls—is related to a change of the permittivity of the medium inside it. The introduced approach turns this principle around and uses for the first time a known permittivity to determine a pressure difference. The resolution in the permittivity was increased subsequently in our publications [12–15]. Here, the noise in the permittivity is



Original content from this work may be used under the terms of the [Creative Commons Attribution 4.0 licence](https://creativecommons.org/licenses/by/4.0/). Any further distribution of this work must maintain attribution to the author(s) and the title of the work, journal citation and DOI.

even further reduced, although this time at the cost of the temporal resolution, resulting in a standard deviation of less than 1 part in 600 million. With that, the diagnostic has become sensitive to such an extent, that the lower detection limit for the pressure differences in ambient air is ~ 0.3 Pa. For the generation of the acoustic waves, the same plasma source was used as in [15] where the electron dynamics in a radio-frequency (RF) driven atmospheric-pressure plasma jet were studied. Moreover, the plasma-induced acoustic waves of a few (tens of) Pa are proposed as an active mechanism in plasma medicine.

2. Microwave cavity resonance spectroscopy

The resonant behaviour of a standing wave in a microwave cavity is described by the spectral position f_{res} and the respective value of the full-width-at-half-maximum Γ of the resonance peak. Changes in the former relate to differences in the real part of the permittivity, while the latter is coupled to the imaginary part. In the past, MCRS was used to study various types of plasmas: pristine RF driven plasmas [16, 17], etching plasmas [18], powder-forming plasmas [19–21], ultracold plasmas [14], EUV photon-induced plasmas [22, 12], and high voltage pulsed [13] and radio-frequency driven [15] atmospheric-pressure plasma jets. Besides for studying plasmas, this technique has been used to determine properties of materials, i.e. molar polarization [23] and dielectric constants in the microwave regime [24].

In this work, the changes in the real part of the permittivity of the material inside the cavity $\Delta\varepsilon$ is investigated and related to transient pressure changes. Hence, only the relative change in the spectral position $\Delta f/f_1$ —with respect to the unperturbed situation—needs to be determined,

$$\frac{\Delta f}{f_1} = -\frac{\iint\int_{V_{\text{cav}}} \Delta\varepsilon |\mathbf{E}_1|^2 d^3\mathbf{r}}{2\varepsilon_0 \iint\int_{V_{\text{cav}}} |\mathbf{E}_1|^2 d^3\mathbf{r}}. \quad (1)$$

In equation (1), \mathbf{E}_1 is the unperturbed spatially dependent electric field of the resonant microwave field, V_{cav} the cavity volume, f_1 the resonance frequency of the unperturbed cavity and ε_0 the vacuum permittivity. The change in permittivity $\Delta\varepsilon$ due to a change in pressure Δp is given by:

$$\Delta\varepsilon = \varepsilon_0 \frac{1 - \varepsilon_{r,1}}{p_1} \Delta p, \quad (2)$$

where $\varepsilon_{r,1}$ is the relative permittivity at pressure p_1 . This equation is rewritten from the Debye equation [23] while assuming that there is no temperature difference and the gas can be described by the ideal gas law, while applying a first-order Taylor expansion around $\varepsilon = 1$. Assuming a cavity homogeneously filled with gas, the two equations above reduce to:

$$\frac{\Delta f}{f_1} = \frac{\varepsilon_{r,1} - 1}{2p_1} \Delta p. \quad (3)$$

At atmospheric pressure, the relative permittivity $\varepsilon_{r,1}$ of He is $1.000\,071 \pm 0.000\,001$ and that of air is $1.000\,575 \pm$

$0.000\,001$ [24] in the microwave range. These values are obtained by the same measurement principal as applied in this publication. Due to recent efforts to increase the resolution in the measured permittivity, this would demonstrate that it is indeed possible to determine these values—even in a temporal manner with ~ 10 μs resolution—with three orders of magnitude better accuracy.

3. Experimental setup and methods

The experimental setup used here comprised a plasma source, a resonant cavity including the required electronics, and equipment for conventional acoustic pressure measurements. A schematic overview of the experimental setup is shown in figure 1. To accommodate the reader, only the essentials of the plasma source and the MCRS setup are given below as they are thoroughly described in [15].

As a plasma source, a pulsed radio-frequency driven atmospheric-pressure discharge was used. These discharges were generated with an excitation frequency of 13.56 MHz in He working gas (purity of 99.999%) flowing at a volumetric rate of 1 slm. A set of two function generators, an RF amplifier and a tunable coil for impedance matching were used to generate plasma. The in-pulse plasma power (~ 20 W) was measured by a multiplying probe [25]. The first function generator was amplitude modulated by a second function generator which was gated by a pulse/delay generator to generate pulsed plasma discharges for a duration of 50 μs (i.e. 678 RF cycles) at a repetition rate of 62.5 Hz. The RF voltage was applied to a vertical needle electrode which was placed concentrically inside a quartz tube (see figure 1). The gas flows from a mixing chamber (I) through 6 parallel channels (II) into a void (III) which was directly connected to the quartz tube (IV) and flows out from the exhaust (V). The cylindrical shell-shaped grounded electrode was placed concentrically around the dielectric tube in a contacting manner while leaving the last 2 mm of the quartz tube uncovered.

A copper cylindrical microwave cavity with an inner diameter of 66 mm and a height of 16 mm was used. A concentric hole of 13 mm in diameter in each of the flat walls allowed the gas flow and discharge to enter and exit the cavity without significantly building up an overpressure. The used TM_{010} mode had a resonance frequency f_{res} of 3.5 GHz and provided a temporal resolution of ~ 1 μs .

A microwave signal with frequency f and power P_{in} (0 dBm) was generated by a microwave generator. These microwaves travelled through a directional coupler and were applied to a straight antenna that protruded a few mm into the cavity. Depending on f , the cavity was able to absorb a certain fraction of P_{in} , and the remainder was reflected through the directional coupler of which -10 dB was directed to a microwave power detector.

To monitor the resonant behaviour, 1401 equidistantly spaced frequencies ranging from 3.509 up to 3.516 GHz were probed. A temperature measurement with sub-mK resolution was performed for each set of f to compensate for thermal

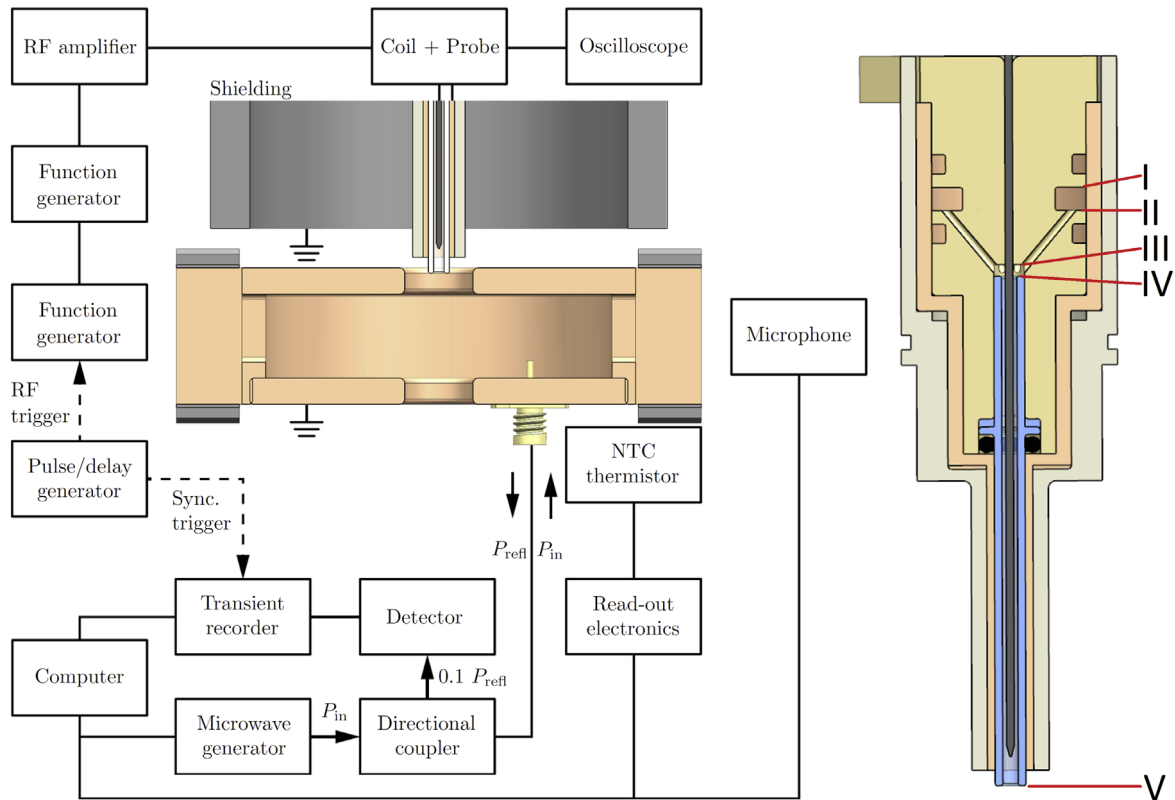


Figure 1. A schematic overview of the experimental setup consisting of the plasma source, cavity including the electronics and the acoustic transducer. The conventional acoustic measurements were performed in the absence of the cavity. On the right side a detailed view of the gas mixing system and quartz tube is shown.

expansion of the cavity [15]. The temporal response of the power detector was sampled at 10 MHz using a transient recorder which was triggered by the same pulse/delay generator to synchronize the measurements with the discharges. The plasma was ignited at $t = 50 \mu\text{s}$ and the period of $10 \mu\text{s}$ directly before the ignition was used to characterize the unperturbed cavity.

Allowed by the extremely high reproducibility of the discharge dynamics, 256 discharges could be used to determine the temporal response at each f to reduce the noise even further, a moving average with a width of 400 timesteps ($40 \mu\text{s}$) was taken of Δf . The cutoff frequency of this low-pass filter was 11 kHz and was optimized for maximum averaging while maintaining bandwidth for frequencies which could fill the cavity ‘homogeneously’. This filter increased the tardiness of the ‘cavity’ and reduced the standard deviation of the noise in the determination of the resonance frequency to 2.8 Hz.

Conventional acoustic measurements were performed for the verification of the MCRS measurements. The transiently varying acoustic pressure was measured by a calibrated transducer, a microphone, of which the output was monitored by a 16-bit ADC at a sample rate of 48 kHz. These measurements were performed at three distances (14, 21 and 28 cm) in the absence of the cavity to prevent additional reflections of the acoustic waves before detection. To increase the signal-to-noise ratio and suppress laboratory background

sounds, from e.g. vacuum pumps and fans, the measured acoustic pressure response was averaged over 256 discharges and synchronized manually with the discharges.

4. Results and discussion

The evolution of the change of the relative resonance frequency $\Delta f/f_1$ is presented in figure 2(a), where the colour black is used to indicate positive shifts and red for negative shifts for visualization. This graph shows that at the end of the pulse period the oscillations in the shift did not vanish in the noise band. This means that the earlier specified value of the noise level is an overestimation. Hence, the characterization of the resonant behaviour of the ‘undisturbed’ cavity contains a small error.

In our previous publication [15] the changes in resonant behaviour during the first $200 \mu\text{s}$ after $t = 0$ were related to the electron dynamics in the discharge. In the $30 \mu\text{s}$ hereafter, the contribution of the electrons to the resonant behaviour was still present. Since this work focuses on acoustic waves, the period during which the plasma contribution dominates the shift/signal is omitted from the analysis. Presumably, free charge carriers do not contribute to changes in the resonant behaviour after $t = 230 \mu\text{s}$. Readers interested in the plasma dynamics are advised to consult our prior publication [15], which discusses the electron dynamics in the spatial afterglow

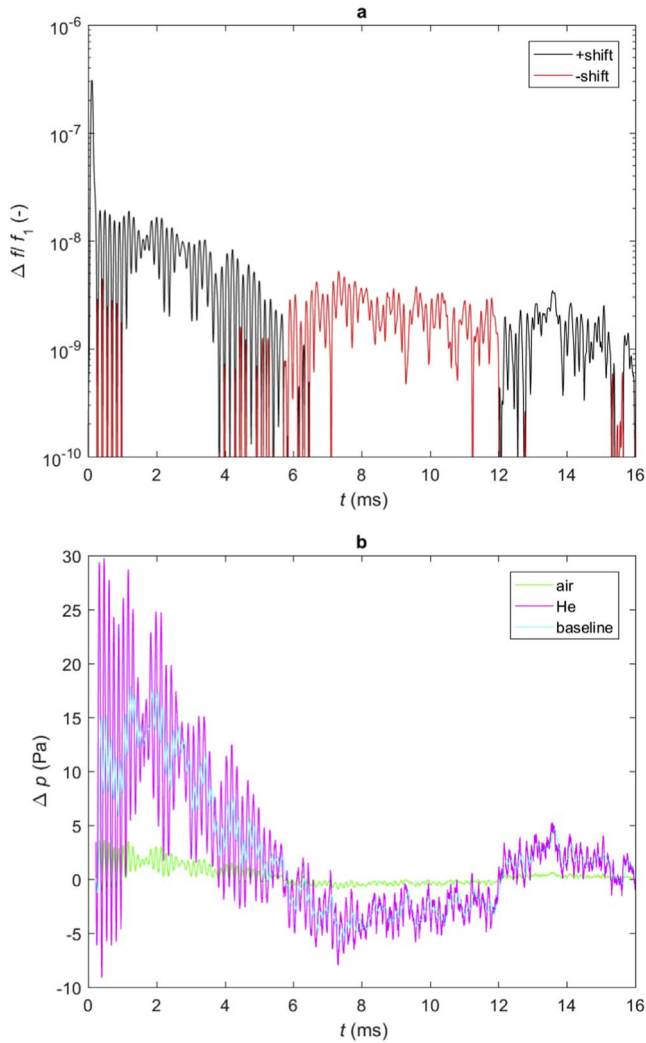


Figure 2. (a) Temporal evolution of the relative frequency shift $\Delta f/f_1$ where the negative values are indicated in red while the positive shifts in black. (b) The pressure difference Δp for air (green) and He (magenta) required to induce a shift in the resonance frequency as presented in (a) are shown.

produced by the same plasma source as used in this investigation.

The obtained shift of the microwave resonance frequency is used to calculate the pressure difference Δp required to induce the shift using equation (3). A graph of the temporal evolution of Δp is shown in figure 2(b) for He (magenta) and air (green). Due to the lower permittivity of He compared to that of air, it requires larger pressure differences to induce the same shift in resonance frequency. This graph shows fast and slow frequency components which were separated by a second moving average with a cutoff frequency of 3.7 kHz. This low-frequency baseline is indicated in the figure with a cyan line. Later in this writing, the low-frequency components, which are attributed to a change in He concentration in the cavity, are discussed in more detail. The fast frequency components, which have been obtained by subtracting the signal with the low-frequency components in the measured signal, are discussed directly below.

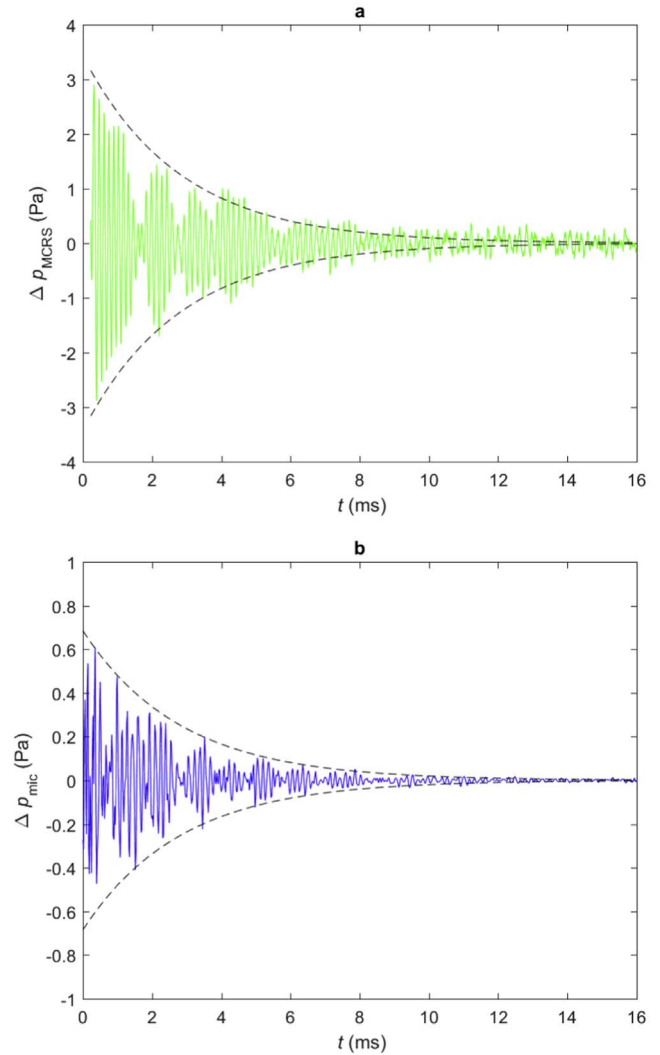


Figure 3. The evolution of the pressure difference obtained by (a) the resonance cavity and (b) the transducer at a distance of 14 cm. The dashed lines are there to guide the eye.

4.1. Acoustic-frequencies components

In the following paragraphs, the results of the MCRS and transducer measurements are compared. In subsequent order, the temporal evolution, the maximum pressure amplitude and the spectral components are described.

4.1.1. Temporal evolution. The transient pressure differences obtained from the MCRS measurements and the acoustic transducer for a distance of 14 cm are shown in figure 3.

The dashed lines are present in the figure to guide the eye. For these lines, exponential decay is assumed following $A \cdot \exp(-B \cdot t)$, where B is equal for both figures and A is scaled to correct for the different measurement positions. Both methods show a decrease in pressure amplitude throughout the first 8 ms after the discharge.

Besides agreement in decay rate, both responses show a pattern related to the superposition of multiple frequencies.

The evolution of pressure Δp_{mic} for the three transducer positions is similar but not identical. This can be explained by

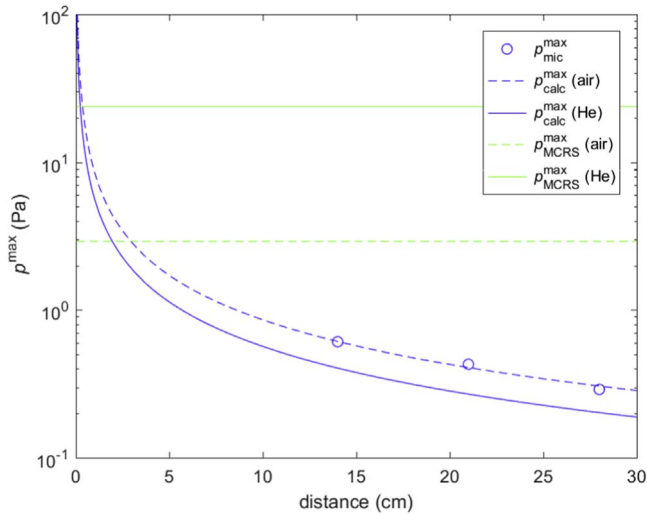


Figure 4. The maximum pressure amplitudes obtained by three methods: the green horizontal lines indicate the required pressure amplitude to induce the measured MCRS shifts, the circles indicate the results from the transducer at the three positions and the blue curved lines represent the amplitudes calculated from the power of the point source. The dashed lines represent the data for air while the solid lines are used for He.

the fact that the plasma source was mounted on a support for the jet and cavity construction which was a suboptimal environment for acoustic measurements due to reflections of the acoustic waves on the metal surfaces.

4.1.2. Pressure amplitude. The maximum pressure amplitudes in the evolution of the transducer measurements $p_{\text{mic}}^{\text{max}}$ on the three positions are used to determine, assuming a point source and conservation of sound intensity, the maximum audio power $P_{\text{max}} = 0.11 \pm 0.01$ mW. Based on P_{max} , the pressure amplitude $p_{\text{calc}}^{\text{max}}$ is calculated for air and He over the relevant range of distances. Figure 4 presents the maximum pressure amplitude obtained by the transducer $p_{\text{mic}}^{\text{max}}$ on the three positions, the calculated $p_{\text{calc}}^{\text{max}}$ and measured by the cavity $p_{\text{MCRS}}^{\text{max}}$. Over this distance range, the maximum pressure amplitude varies from 0.2 up to 100 Pa. For reference, a pressure amplitude of 1 Pa equals a sound pressure level of 94 dB. Note that the measured sound levels can induce hearing damage.

Near the point source, the pressure amplitude $p_{\text{calc}}^{\text{max}}$ is relatively large while the MCRS sensitivity here is low as the gas in this region consists mainly of He. The abscissa of the intersection of the lines $p_{\text{MCRS}}^{\text{max}}$ and $p_{\text{calc}}^{\text{max}}$ is 0.2 cm for He and 2.9 cm for air. As the former is approximately the radius for the region of the He gas flow and the latter the inner cavity radius, the maximum pressure amplitudes obtained by the cavity and transducer are in good agreement with each other.

4.1.3. Frequency analysis. A Fourier transform algorithm is used for the spectral analysis of the transient pressures. The

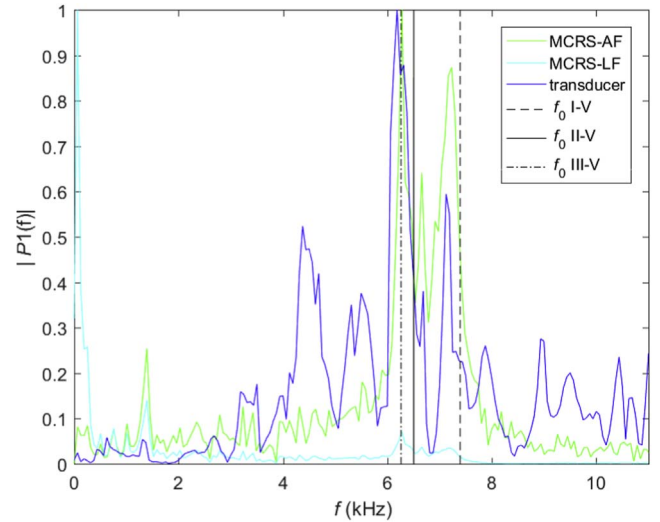


Figure 5. Normalized spectral densities of the responses obtained by MCRS and transducer measurements. MCRS-AF and MCRS-LF are the spectra of the signal with acoustic-frequency components and low-frequency components, respectively. The black vertical lines indicate the calculated acoustic resonance frequencies f_0 .

spectra for the MCRS and transducer at a distance of 14 cm are presented in figure 5.

The transducer spectrum contains peaks which are not present in the MCRS spectrum. This difference is attributed to the higher sensitivity of the transducer with respect to laboratory sounds due to its placement and omnidirectional sensitivity. Further, the higher-frequency waves might cancel out in the volume of the cavity. The spectral positions of the three most prominent peaks of the high-frequency components, indicated in green, are very close to the related peaks in the transducer's spectrum (blue). To find the cause of the acoustic waves and the mechanism behind them, the spectrum is further analyzed. The resonance frequency f_0 of an acoustic wave in a tube with both ends open is given by:

$$f_0 = \frac{vn_0}{2L}, \quad (4)$$

where v is the speed of sound, n_0 is the resonant mode number and L is the length of the pipe.

The geometry of the quartz tube and mixing chamber is rather complex making it difficult to identify the corresponding parts which act as an acoustic column. The total distance from the exhaust of the quartz tube (IV) up to the end part (I, II or III) is used to define L . The length L and its estimated error are given in table 1 for three combinations of parts of the source geometry.

The transducer spectrum contains peaks which are not present in the MCRS spectrum. This difference is attributed to the higher sensitivity of the transducer with respect to laboratory sounds due to its placement and omnidirectional sensitivity.

The spectral positions of the peaks in the MCRS and transducer spectra which are related to these theoretical spectral positions of f_0 for $n_0 = 1$ are presented in the same table and in figure 5 by the vertical lines. These

Table 1. The resonance frequencies measured and calculated for several combinations of parts of the discharge geometry are presented in the table. The parts are identified by Roman numerals in the first column while the length of the source geometry L is given in the second column. The corresponding acoustic resonance frequencies are presented in the other columns.

parts	L (m)	f_o (kHz)	f_{MCRS} (kHz)	f_{mic} (kHz)
I–V	0.0830 ± 0.0002	6.3 ± 0.2	6.19 ± 0.06	6.28 ± 0.06
II–V	0.0780 ± 0.0002	6.5 ± 0.2	6.69 ± 0.06	6.66 ± 0.06
III–V	0.0680 ± 0.0002	7.4 ± 0.2	7.13 ± 0.06	7.23 ± 0.06

experimentally and theoretically determined spectral positions are in good agreement with each other. For this reason, the acoustic pressure waves that are detected, can be attributed to standing waves in the gas delivery system.

Hence, these frequencies can be tuned by adjusting the length of the tubes to induce acoustic resonances at a specific resonance frequency, i.e. to prevent intermixing of the contributions of the electron dynamics and acoustic resonances during MCRS measurements.

4.2. Low-frequency components

The low-frequency components, which were separated by the second moving average filter, are treated from here on. These disturbances consist mainly of components with frequencies below 250 Hz, as indicated in cyan in figure 5, and were not detected by the transducer. As these oscillations fell within the measurement range of the apparatus, it suggests that these are not related to an acoustic wave phenomenon.

The measured shift of the resonance frequency is caused by a change in cavity content, e.g. the He/air ratio. Based on the relative resonance frequency shift, the required change of the E-field-weighted He content in the cavity is estimated as 1 part in 10^5 . As this is only 0.5 mm^3 of the air replaced by He and vice versa, it is plausible. These oscillations were not damped within the pulse period of 16 ms which means that the previous discharge still affects the dynamics of consecutive discharges after 16 ms. This might be an alternative explanation for the found trend in the height of the jump in electron density after turning off the RF power in our previous publication [15].

5. Conclusions and outlook

The temporal evolution, the pressure amplitude and spectra of the MCRS and transducer measurements are in good agreement with each other. Less prominent peaks in the transducer spectrum are not present in the MCRS spectrum, which can be explained by the absence of the cavity during the transducer measurements and high-frequency waves can be averaged out in the cavity volume.

Low-frequency components in the MCRS spectrum are attributed to a change in the gas composition in the cavity and are proposed as an alternative explanation of a plasma phenomenon described in our previous publication [15].

No audible sound was observed when the plasma was not pulsed, which suggests that the acoustic waves are produced

during the generation or decay of the plasma. This observation supports the work of Lietz [8].




Plasma-induced shock waves are used for many years in plasma medicine, however at elevated levels—500 Pa up to 100 MPa [26–28]—in comparison to the pressure differences measured here. As only a few Pa is sufficient to cause ruptures of biopolymers within cells [29], it is very much possible that these milder shock waves could be an active mechanism in plasma medicine.

Earlier in this communication, it was stated that the accuracy in measuring the real part of the permittivity was increased by 3 orders of magnitude compared to Birnbaum *et al* [24]. In contrast to the experiment presented here which required large holes in the cavity, for the determination of the permittivity of gasses, a cavity with small holes suffices. This cavity will have lower losses and higher resolution in the real part of the permittivity. Moreover, investigating non-transient resonant behaviour requires less time and therefore allows for more averaging and smaller frequency steps. Both contribute to a further increase in the resolution making this a competitive technique for the determination of material properties.

The introduced approach could also be applied in the following experiment which makes use of the unique feature of the MCRS technique: the capability of probing pressure differences without direct access. By doing this up- or downstream of a plasma confined to a glass tube, it would be possible to determine the product of the gas-heating volume and the change of gas temperature without the need to separate the acoustic waves from the electron dynamics. As this process of gas-heating takes place within tens of ns, so far no other experimental methods are available to study these phenomena [8]. By reducing the height of the cavity and the diameter of the axial holes, a larger range of acoustic frequencies would satisfy the conditions of the uniformly filled probing volume. Moreover, this experiment would benefit from the approach to correct the resonant field for the presence of the glass tube introduced by Faltýnek *et al* [17] and to spatially resolve the pressure gradients by using multiple resonant modes [12].

In summary, these results demonstrate that microwave cavity resonance spectroscopy can be used to study acoustic pressure waves. In contrast to Schlieren imaging and acoustic measurements, the approach introduced in this work is capable of resolving transient pressure differences over longer timescales and volumes even without direct access. The pressure waves induced by the plasma can be described as standing waves in the tube of the plasma jet configuration.

ORCID iDs

B Platier  <https://orcid.org/0000-0003-4524-0131>
 T J A Staps  <https://orcid.org/0000-0002-9859-2942>
 J Beckers  <https://orcid.org/0000-0001-6116-7013>

References

- [1] Foest R, Kindel E, Lange H, Ohl A, Stieber M and Weltmann K D 2007 *Contrib. Plasma Phys.* **47** 119–28
- [2] Penkov O V, Khadem M, Lim W S and Kim D E 2015 *J. Coat. Technol. Res.* **12** 225–35
- [3] Brandenburg R, Ehlbeck J, Stieber M, Woedtke T V, Zeymer J, Schlüter O and Weltmann K D 2007 *Contrib. Plasma Phys.* **47** 72–9
- [4] Winter J, Brandenburg R and Weltmann K D 2015 *Plasma Sources Sci. Technol.* **24** 064001
- [5] Sasaki S, Kanzaki M and Kaneko T 2014 *Appl. Phys. Express* **7** 026202
- [6] Keidar M, Yan D, Beilis I I, Trink B and Sherman J H 2018 *Trends Biotechnol.* **36** 586–93
- [7] Kong M G, Kroesen G M W, Morfill G, Nosenko T, Shimizu T, Van Dijk J and Zimmermann J L 2009 *New J. Phys.* **11** 115102
- [8] Lietz A M, Johnsen E and Kushner M J 2017 *Appl. Phys. Lett.* **111** 114101
- [9] Xian Y B, Hasnain Qaisrani M, Yue Y F and Lu X P 2016 *Phys. Plasmas* **23** 103509
- [10] Whalley R D and Walsh J L 2016 *Sci. Rep.* **6** 1–7
- [11] Zhao W, Tian K, Tang H, Liu D and Zhang G 2002 *J. Phys. D: Appl. Phys.* **35** 2815–22
- [12] Beckers J, van de Wetering F M J H, Platier B, van Nindhuijs M A W, Brussaard G J H, Banine V Y and Luiten O J 2019 *J. Phys. D: Appl. Phys.* **52** 034004
- [13] Van Der Schans M, Platier B, Koelman P M J, Van De Wetering F M J H, Van Dijk J, Beckers J, Nijdam S and IJzerman W L 2019 *Plasma Sources Sci. Technol.* **28** 035020
- [14] Van Nindhuijs M A W, Daamen K A, Franssen J G H, Conway J, Platier B, Beckers J and Luiten O J 2019 *Phys. Rev. A* **100** 061801
- [15] Platier B, Staps T J A, Van Der Schans M, IJzerman W L and Beckers J 2019 *Appl. Phys. Lett.* **115** 254103
- [16] Franek J, Nogami S, Koepke M, Demidov V and Barnat E V 2019 *Plasma* **2** 65–76
- [17] Faltýnek J, Kudrle V, Tesar J, Volfová M and Tálský A 2019 *Plasma Sources Sci. Technol.* **28** 105007
- [18] Stoffels E, Stoffels W W, Vender D, Kando M, Kroesen G M W and De Hoog F J 1995 *Phys. Rev. E* **51** 2425–35
- [19] Beckers J, Stoffels W W and Kroesen G M W 2009 *J. Phys. D: Appl. Phys.* **42** 155206
- [20] Wattieaux G, Carrasco N, Henault M, Boufendi L and Cernogora G 2015 *Plasma Sources Sci. Technol.* **24** 015028
- [21] Alcouffe G, Cavarroc M, Cernogora G, Ouni F, Jolly A, Boufendi L and Szopa C 2010 *Plasma Sources Sci. Technol.* **19** 015008
- [22] Van Der Horst R M, Beckers J, Nijdam S and Kroesen G M W 2014 *J. Phys. D: Appl. Phys.* **47** 7–11
- [23] Magnuson D W 1956 *J. Chem. Phys.* **24** 344–7
- [24] Birnbaum G, Kryder S J and Lyons H 1951 *J. Appl. Phys.* **22** 95–102
- [25] Beijer P A C, Sobota A, Van Veldhuizen E M and Kroesen G M W 2016 *J. Phys. D: Appl. Phys.* **49** 104001
- [26] Chan K F, Pfefer T J, Teichman J M H and Welch A J 2001 *J. Endourol.* **15** 257–73
- [27] Lukes P et al 2014 *Shock Waves* **24** 51–7
- [28] Roth C C, Maswadi S, Ibey B L, Beier H T and Glickman R D 2014 *Optical Interactions with Tissue and Cells XXV; and Terahertz for Biomedical Applications* vol 8941894110
- [29] Suresh S 2007 *Acta Mater.* **55** 3989–4014